Applied Catalysis B: Environmental 91 (2009) 39–46

Contents lists available at ScienceDirect

Applied Catalysis B: Environmental

journal homepage: www.elsevier.com/locate/apcatb

W-doped titania nanoparticles for UV and visible-light photocatalytic reactions

Olivier Lorret [a,*], Denisa Francová [b], Georg Waldner [a], Nils Stelzer [a]

[a] Advanced Materials and Aerospace Technologies, Austrian Research Centers GmbH-ARC, A-2444 Seibersdorf, Austria
[b] Vienna University of Technology, Institute of Materials Chemistry, Getreidemarkt 9-165, A-1060 Vienna, Austria

ARTICLE INFO

Article history:
Received 14 October 2008
Received in revised form 24 April 2009
Accepted 1 May 2009
Available online 9 May 2009

Keywords:
Sol–gel Ti(W)O_x photocatalysts
Nanoparticles
Visible light
Methylene blue

ABSTRACT

Nanocrystalline tungsten doped titanium dioxide powders were prepared by a sol–gel method based on hydrolysis of $TiCl_4$ in aqueous solution. Addition of W was done to extend light absorption of the TiO_2-based photocatalysts towards the visible light range. Different tungsten precursors and contents were investigated, regarding their photocatalytic properties and activity. Their photocatalytic activity was measured via degradation of methylene blue (MB) in aqueous solution under ultraviolet (UVA) or visible light. Highest activity was observed for sol–gel samples calcined at 773 K, due to full removal of chloride and increase of crystallite size by thermal treatment. Activity of Ti(W)O_x sol–gel photocatalysts under UVA strongly depends on the tungsten content (maximum reached for a ratio between 1 and 2 mol%) and the precursor choice ($WCl_6 > (NH_4)_6H_2W_{12}O_{40} > H_2WO_4$). Under visible-light, activity increases with W content.

1. Introduction

Titanium dioxide is one of the most important and widely investigated photocatalysts because of its optical and electronic properties, low cost, chemical stability, non-toxicity [1–4] and potential application in decomposition of many organic pollutants present in liquid effluents [5–8] or in gaseous phases [9,10]. Natural polymorphs of TiO_2 are known to exist as tetragonal rutile and anatase or orthorhombic brookite [11–14]. Titanium dioxide is generally obtained either from minerals, gas phase reactions or from a solution of titanium salts or alkoxides through thermolysis, hydrothermal processes [15,16] or sol–gel method [17,18]. The photoactivity of TiO_2 is strongly dependent on its crystalline structure, crystallite size, surface morphology and synthesis method used [1,19,20].

In the last decades, the sol–gel method has gained increasing attention for the preparation of nanoparticles, due to the inexpensive equipment required, low temperature involved and the possibility to have a direct control on various material parameters such as phase structure, crystallinity, average nanocrystallite size and surface area.

Generally, TiO_2 is only sensitive to UV radiation due to its large band gap (3.2 eV) [21]. Sun light is an abundant photon source, of which, unfortunately, the UV radiation is only a small fraction (~5%) compared to the visible region (45%). Recently, considerable efforts have been made to develop doped TiO_2 in order to extend the absorption spectrum to visible light and thus harvest solar energy more efficiently for practical applications. Several authors reported doping TiO_2 with non-metallic elements, such as nitrogen, carbon, fluorine, sulphur, [22–25] or transition metals [1,26–28]. Some recent publications report a significant improvement of photocatalytic activity in the degradation of organic compounds in aqueous systems with tungsten doped titanium dioxide [29–32] or as photocatalytic catalyst for water cleavage [33]. An explanation for this enhancement can be found in the suitable distribution of energy levels of valence and conduction bands of TiO_2 and WO_3, respectively, cf. Scheme 1 [34]: in case of electronic contact of separate oxide phases, the charge separation process is facilitated by removal towards the energetically lower-lying bands of the partner oxide; also in case of substitutional doping by higher-valence cations, there is an alteration of the electronic structure of the main semiconductor (TiO_2), which assists the charge separation efficiency.

However a comparison among the results reported in the literature for doped TiO_2 photocatalysts is not easy because of the various tungsten sources (H_2WO_4, $(NH_4)_6H_2W_{12}O_{40}$, WCl_6, $W(OEt)_5$, etc.) [35–38], the different techniques for doping (impregnation, sol–gel, flame spray synthesis, etc.) [31,39–41], products of unknown purity and other unidentified parameters as well as the different photocatalytic tests and experimental conditions used.

In this work, nanosized TiO_2 and Ti(W)O_x powder were prepared by a sol–gel process based on hydrolysis of $TiCl_4$ in aqueous solution [42]. Different tungsten precursors and different chemical compositions were used for the photocatalysts preparation. Their effects as well as the effect of calcination temperature on activity in the decomposition of the cationic dye methylene blue (MB) under

* Corresponding author. Tel.: +43 050 550 2734; fax: +43 050 550 3366.
E-mail address: olivier.lorret@arcs.ac.at (O. Lorret).

0926-3373/$ – see front matter © 2009 Elsevier B.V. All rights reserved.
doi:10.1016/j.apcatb.2009.05.005

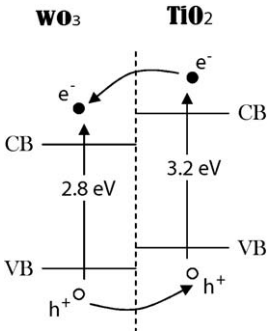

Scheme 1. Schematic representation of energy levels of valence and conduction bands in TiO_2 and WO_3.

exposure to both ultraviolet (UVA) and visible light radiation in an aqueous solution were investigated.

2. Experimental

2.1. Materials

The nanocrystalline TiO_2 and $Ti(W)O_x$ powders containing 1, 2 and 5 mol% tungsten were synthesized via a sol–gel process using the hydrolysis and the condensation of titanium tetrachloride in an aqueous medium. For this purpose, 10 mL $TiCl_4$ (Aldrich, 99.9%) was slowly added to 100 mL distilled water (molar ratio Ti:H_2O 1:60) at room temperature. A second solution with the required amounts of $(NH_4)_6H_2W_{12}O_{40}$ (Alfa Aesar, 99%), H_2WO_4 (Acros Organics, 99%) or WCl_6 (Acros Organics, 99.9%) in 50 mL H_2O, 2.5 M NH_4OH aqueous solution or ethanol, respectively, was added to the clear $TiCl_4$ solution. After 15 h of continuous stirring at room temperature (RT), the reaction mixture was diluted with H_2O until the desired Ti:H_2O molar ratio of 1:300 [42]. The resulting clear solution was heated 1.5 h at 353 K. The characterization of all samples was carried out on the powders obtained by drying the dispersion at 353 K. The following codes were used for the samples: TiO_2, $Ti(W)O_x$-A(n), $Ti(W)O_x$-B(n), $Ti(W)O_x$-C(n), where A, B or C indicate the W precursor, $(NH_4)_6H_2W_{12}O_{40}$, H_2WO_4 or WCl_6, respectively and n indicate the molar percentage (%) of W.

2.2. Sample characterizations

The X-ray powder diffraction patterns (XRD) were obtained with a Philips X'Pert diffractometer using Cu Kα radiation (λ = 1.5417 Å, 40 kV and 45 mA). Specific surface areas were determined by N_2 adsorption (BET method) at 77 K with a Micromeritics ASAP 2020 apparatus on samples calcined in synthetic air at 723 K and outgassed at RT and 10^{-4} Pa. High resolution transmission electron microscopy HRTEM and EDX line scan measurements were performed on a Philips TECNAI F20 (USTEM, Vienna University of Technology). Samples were prepared by dispersing the particles in ethanol prior to deposition on a SiO_2 coated TEM Cu grid. The Raman spectra were recorded by a Horiba Jobin-Yvon Labram Aramis FT-Raman spectrophotometer. The UV–vis diffuse reflectance spectra were obtained on pellets calcined 15 h at 773 K with an Ocean Optics DH-2000-BAL D_2/W lamp, a fiber optic reflection probe and a USB4000 detector.

2.3. Photocatalytic reactions

The photocatalytic activity of the sol–gel nanocrystalline TiO_2 and $Ti(W)O_x$ powders was studied by monitoring the degradation of the MB in an aqueous solution containing the nanocrystalline powders, under continuous stirring and exposure to the ultraviolet (UVA) or visible light radiation. The photocatalytic degradation of MB was performed as follows: a Pyrex photoreactor was filled with 200 mL of aqueous solution of 20 μM MB, and 0.05 g of catalyst (0.25 g/L) open to the atmosphere. The resulting suspension was adjusted at pH = 4 with HNO_3 or NH_4OH. A pH value of 4 was chosen and fixed because it is close to the natural pH of the different powders and to make the comparison of samples activity easier. Indeed, adsorption of MB at the surface of the TiO_2 nanoparticles is strongly dependant of the pH. A quite basic pH will favor adsorption of MB and activity while a more acidic pH will decrease adsorption of MB due to the presence of cationic species at the surface of the particles and decrease their photocatalytic activity [43]. Then the solution was equilibrated by stirring in the dark for 0.5 h to stabilize the adsorption of the MB dye over the surface of the nanocrystalline photocatalysts.

The stable aqueous suspensions were irradiated with UV or visible light, under continuous magnetic stirring, using an aluminum chamber thermostated at 293 K containing two 9 W UVA black light bulbs (Sylvania UVA-BLB Lynx S) or daylight fluorescent (Osram Dulux S 860) tubes. The emission spectra of the lamps used throughout this study are shown in Fig. 1. The daylight fluorescent tubes show a small UV emission peak; quantification of UV and visible light intensities are given in Table 1. The latter were determined by use of a Vilber Lourmat VLX-3W 365 nm (±10 nm) detector; lamp emission spectra were integrated over the desired wavelength range (300 nm to 400 nm or 400 nm to 500 nm). The following ratio was used to recalculate the irradiance values I [mW cm^{-2}]:

$$I_{(300-400\,\mathrm{nm})} = \frac{I_{(\mathrm{detector},\,355-375\,\mathrm{nm})} * A_{(\mathrm{spectrum},\,300-400\,\mathrm{nm})}}{A_{(\mathrm{spectrum},\,355-375\,\mathrm{nm})}}$$

Light intensities [E s^{-1} cm^{-2}], E being the symbol for Einstein (mol photons) were calculated as follows:

$$\mathrm{Int.} = \frac{I}{1000 * h * \nu * N_A}$$

The UV intensity of the daylight lamps cannot account for the observed visible light degradation, as the efficiency with Degussa P25 is not measurable under the same type of daylight lamp.

The degradation was monitored by sampling at various time intervals. The clear solutions obtained after centrifugation of the samples were examined using UV–vis spectroscopy to study the degradation of the MB dye. The absorption spectra of the MB dye solution were obtained within the range of 400–900 nm as a function of radiation exposure time. The intensity of absorbance peak (A) of the MB dye solution, located at λ = 665 nm was taken as a measure of the residual concentration of MB dye (C). The UV–vis absorbance spectrum of the solution, prior to the radiation exposure, was also recorded as a reference spectrum corresponding to the initial MB dye concentration (C_0). The normalized residual concentration of MB dye was then obtained using the relationship of the form

$$\left(\frac{C}{C_0}\right)_{\mathrm{MB}} = \left(\frac{A_t}{A_{t=0}}\right)_{665\,\mathrm{nm}}$$

3. Results and discussion

XRD patterns of pure TiO_2 and doped $Ti(W)O_x$ (100:2 molar ratio) samples calcined at 773 K for 15 h are shown in Fig. 2. The pure TiO_2 sample presents a main reflection peak at $2\theta = 25.4^\circ$ characteristic of anatase phase and traces of a reflection peak at $2\theta = 27.6^\circ$ characteristic of rutile phase. For all $Ti(W)O_x$ samples, no other phases than anatase were detected, it could be concluded that some Ti^{4+} in the lattice of TiO_2 are substituted by W^{n+} ($4 < n < 6$). Indeed, the ion radius of W^{n+} (0.62–0.70 Å) and Ti^{4+} (0.68 Å) are quite similar. The lattice strains of the samples

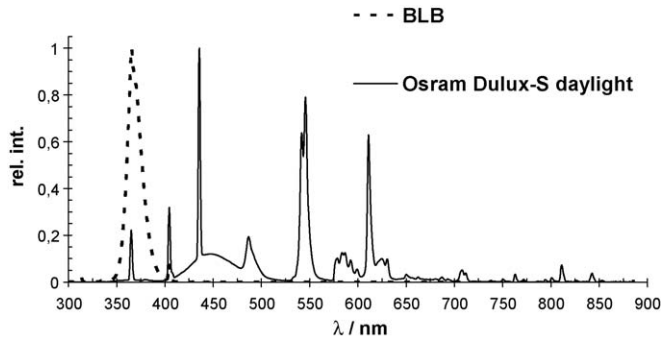

Fig. 1. Relative emission spectra of 9 W UVA-BLB and visible-light lamps.

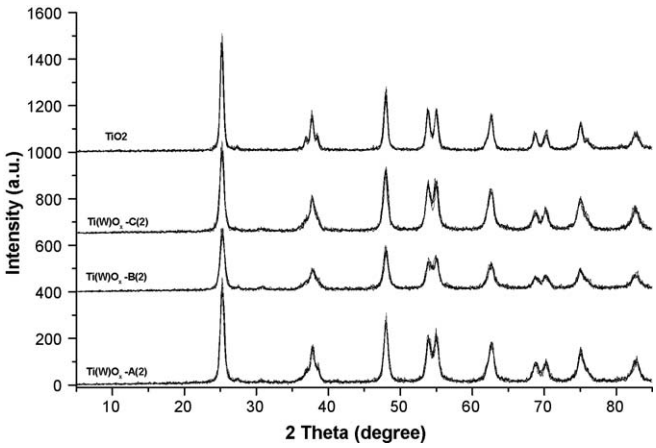

Fig. 2. XRD patterns of pure anatase TiO_2 and doped Ti(W)O_x (100:2 molar ratio) samples calcined 15 h at 773 K.

measure from XRD are reported in Table 2. The small change in the lattice strain observed at increasing W amount can be an indication of a progressive incorporation of the W atoms in the lattice of TiO_2. The peak broadening was used to calculate the crystallite size of the anatase phase, applying Scherrer's formula. Table 2 reports the nomenclature and some of the textural properties of the samples calcined at 773 K such as crystallite size of primary particles and specific surface areas (SSA). Independently of the nature of the precursor, the addition of W in the TiO_2 samples decreases the crystallite size, from 21 to ~15 nm, and considerably increases SSA, from 16 to ~50 m^2/g. Tungsten content plays an important role within one series with the same W precursor. Indeed an increase of the W ratio from 1 to 5 mol% decreases the crystallite size of particles and increases the SSA of the powder. The lowest crystallite size is obtained for the series using H_2WO_4 as tungsten precursor dissolved in ammonia solution. The addition of a basic solution to an acidic medium changes the natural pH of hydrolyzed $TiCl_4$ solution which can explain the decrease of the particle growth via alteration of nucleation and growth rate.

Fig. 3 shows the XRD pattern of Ti(W)O_x-A(2) as prepared and calcined at different temperatures between 573 and 873 K. The same behavior is observed for all the Ti(W)O_x samples. The as prepared sample presents broad diffraction peaks, the anatase phase is observed with traces of brookite. The diffraction peaks of the samples become more intense and sharper by increasing the calcination temperature of the samples from 573 to 873 K indicating that the crystallite size of the particles increased. It is important to note that the sample calcined at 873 K shows only diffraction peaks corresponding to the anatase phase. Table 3 displays the crystallite size of the primary particles and the SSA of Ti(W)O_x-A(2) as prepared and calcined. It can be noted that the growth of particle size is accompanied by a constant decrease of SSA when the calcination temperature increase. No rutile phase formation is detected for samples calcined up to 873 K (which is usually given as starting temperature of rutile formation), but a drastic increase of the crystallite size and a decrease of SSA are observed.

The Raman spectra recorded at RT of TiO_2 and Ti(W)O_x samples calcined at 773 K are reported on Fig. 4. The Ti(W)O_x-A series (1–5 mol% of W) is representative of all the TiO_2/WO_3 samples. Both samples show peaks at 145 (E_g), 198 (E_g), 399 (B_{1g}), 522 ($A_{1g} + B_{1g}$) and 639 cm^{-1} (E_g) which are directly attributable to anatase phase [44]. Pure TiO_2 sample presents also a shoulder at 447 cm^{-1} (E_g) which is attributable to rutile phase present in small quantity as reported on XRD spectra. The Raman spectrum for the pure WO_3 oxide (not shown) present sharp peaks at 309 (O–W–O bending),

Table 1
Light flux values employed for photocatalytic studies; irradiance in mW cm^{-2}, intensity in E s^{-1} cm^{-2} (E = Einstein = mol photons).

Lamp	UV light flux (300–400 nm)		VIS light flux (400–500 nm)	
	mW cm^{-2}	E s^{-1} cm^{-2}	mW cm^{-2}	E s^{-1} cm^{-2}
2× Sylvania BLB (9 W)	3.2	9.9×10^{-9}	0.07	1.6×10^{-10}
2× Osram Dulux S 860 (9 W)	0.21	6.5×10^{-10}	3.4	7.6×10^{-9}

Table 2
Textural characteristics and photocatalytic activities in the MB degradation of TiO_2 and Ti(W)O_x samples calcined 15 h at 773 K.

Samples	W precursor	W content (mol%)	Crystallite size (nm)[a]	Lattice strain (%)[a]	S_{BET} (m^2/g)[b]	k_{UVA} (s^{-1})[c]	k_{VIS} (s^{-1})[c]
TiO_2	–	–	20.6	0.92	16	1.9×10^{-4}	0
Ti(W)O_x-A(1)	$(NH_4)_6H_2W_{12}O_{40}$	1	16.3	1.12	57	5.8×10^{-4}	6.9×10^{-5}
Ti(W)O_x-A(2)	$(NH_4)_6H_2W_{12}O_{40}$	2	13.9	1.33	58	5.9×10^{-4}	8.8×10^{-5}
Ti(W)O_x-A(5)	$(NH_4)_6H_2W_{12}O_{40}$	5	12.0	1.46	67	3.7×10^{-4}	6.1×10^{-5}
Ti(W)O_x-B(1)	H_2WO_4	1	14.8	1.22	46	3.7×10^{-4}	4.8×10^{-5}
Ti(W)O_x-B(2)	H_2WO_4	2	12.9	1.37	52	3.3×10^{-4}	5.3×10^{-5}
Ti(W)O_x-B(5)	H_2WO_4	5	9.7	1.77	68	2.5×10^{-4}	5.9×10^{-5}
Ti(W)O_x-C(1)	WCl_6	1	16.1	1.12	46	4.9×10^{-4}	5.6×10^{-5}
Ti(W)O_x-C(2)	WCl_6	2	14.5	1.24	54	7.4×10^{-4}	8.1×10^{-5}
Ti(W)O_x-C(5)	WCl_6	5	11.6	1.52	72	2.9×10^{-4}	9.5×10^{-5}

[a] Calculated by XRD.
[b] BET specific surface areas determined on samples calcined at 723 K and outgassed at RT.
[c] Pseudo-first order reaction rate constant.

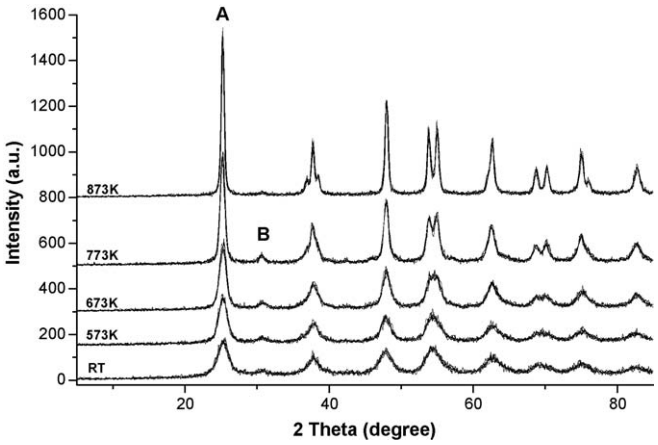

Fig. 3. XRD patterns of Ti(W)O_x-A(2) sample as-prepared and calcined 15 h at 573 K, 673 K, 773 K and 873 K.

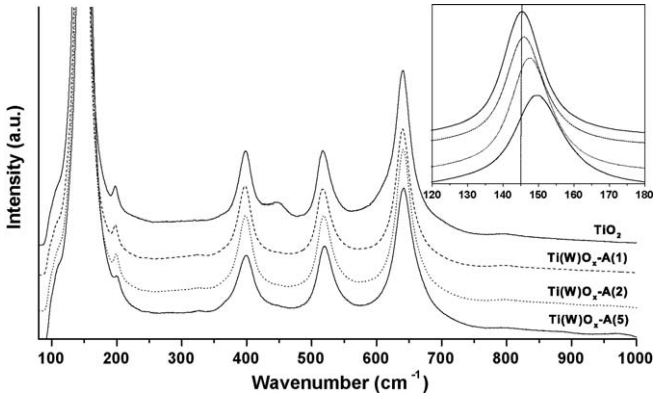

Fig. 4. Raman spectra of sol–gel TiO_2 and Ti(W)O_x-A series powders calcined 15 h at 773 K, (inset) zoom in the region 120–180 cm^{-1}.

808 (O–W–O stretching) and 924 cm^{-1} (terminal W=O stretching)[45,46]. The detection of Raman bands of WO_3 at 309 and 808 cm^{-1} is difficult, because they are overlapped by a strong, broad background signal of anatase. The Raman spectrum for the Ti(W)O_x-A series are identical to anatase, there are no additional peaks detected in the region 900–1000 cm^{-1}. This clearly indicates that tungsten species are uniformly dispersed in the titania nanoparticles. There is also a shift in the anatase Raman main peak at 145 cm^{-1}, Fig. 4b. Indeed this peak is red-shifted at increasing tungsten loading, indicating an incorporation of the tungsten in the lattice of the TiO_2.

HRTEM images in Fig. 5 reveal that the TiO_2 and Ti(W)O_x samples calcined at 773 K consist of agglomerates of primary particles of 10–20 nm in diameter, which is in good agreement with the XRD calculation. The uniform lattice fringes of anatase TiO_2 can be observed over an entire primary particle and no WO_3 clusters are found around titania. Fig. 5e and f shows the amount of Ti and W, respectively, through one particle of Ti(W)O_x-C(2), cf. line scan (Fig. 5d) performed by EDX. The distribution of W in this particle, like in all the Ti(W)O_x particles prepared in this study, follows the distribution of Ti with respect to different intensity of the elements and some experimental errors due to the low W loading. This general trend supports the hypothesis of a homogeneous dispersion of tungsten into the TiO_2 nanocrystallite as suggested by XRD and Raman spectroscopy.

Fig. 6 shows the diffuse reflectance spectra of Ti(W)O_x-A series (1–5 mol% of W) powder, representative of all the TiO_2/WO_3 series, calcined at 773 K. The spectra of sol–gel TiO_2 and pure WO_3 powders were also included in this figure for comparison. The absorption band edge of pure WO_3 (around 415 nm) is red-shifted by 50 nm compared to the sol–gel TiO_2 powder. The spectra of the loaded samples show a slight red-shift in the band edge, the extent depends on the tungsten loading. The absorbance in the visible region is always higher than that of the sol–gel TiO_2 reference.

Fig. 7a shows the typical UV–vis absorbance spectra obtained for the MB degradation under UVA irradiation for different time intervals. It can be noted that the intensity of the main peak at λ_{max} = 665 nm is decreasing continuously with increasing irradiation time, showing the photocatalytic degradation of the MB organic dye in presence of pure TiO_2 or doped Ti(W)O_x sol–gel samples. It is well known that the photocatalytic degradation of organic dyes like MB follows the Langmuir–Hinshelwood kinetics, which may be expressed as [1,47]

$$-\frac{dC}{dt} = kC$$

where dC/dt is the rate of change in the organic dye concentration, t the UV radiation exposure time, k the first-order reaction rate constant, and C the concentration of the organic dye. The latter equation can be linearized by taking the logarithm as

$$\ln\left(\frac{C_0}{C}\right) = kt$$

where C_0 is an initial organic dye concentration. The first order reaction rate constant k is a direct indication of the photocatalytic activity of the different powder photocatalysts [6,48], and can be determined from the slope of the graph $\ln(C_0/C)$ versus time as shown in Fig. 7b.

First, the influence of calcination temperature on MB photocatalytic degradation for Ti(W)O_x-A(2) was studied. The general trend observed in Fig. 8 is representative of all the sol–gel samples. The as prepared sample presented an activity lower than the limit

Table 3
Textural characteristics and photocatalytic activities in the MB degradation of Ti(W)O_x-A(2) samples calcined 15 h at different temperatures.

Calcination temperature (K)	Crystallite size (nm)[a]	S_{BET} (m^2/g)[b]	[Cl^-] (mol L^{-1})[c]	k_{UVA} (s^{-1})[d]	k_{VIS} (s^{-1})[d]
353	4.9	217	3.16×10^{-4}	<l.d.	<l.d.
573	6.2	141	1.05×10^{-5}	3.3×10^{-5}	<l.d.
573 wash[e]	6.2	141	4.07×10^{-6}	2.9×10^{-4}	–
673	8.4	95	1.41×10^{-6}	3.6×10^{-4}	3.8×10^{-5}
773	13.9	58	1.02×10^{-6}	5.9×10^{-4}	8.8×10^{-5}
773 wash[e]	13.9	58	9.77×10^{-7}	5.8×10^{-4}	–
873	22.9	33	9.33×10^{-7}	2.9×10^{-4}	6.0×10^{-5}

[a] Calculated by XRD.
[b] BET specific surface areas determined on samples outgassed at RT.
[c] Determined for 50 mg of powder in 100 mL distilled water.
[d] Pseudo-first order reaction rate constant.
[e] Photocatalysts washed several times in water before calcination.

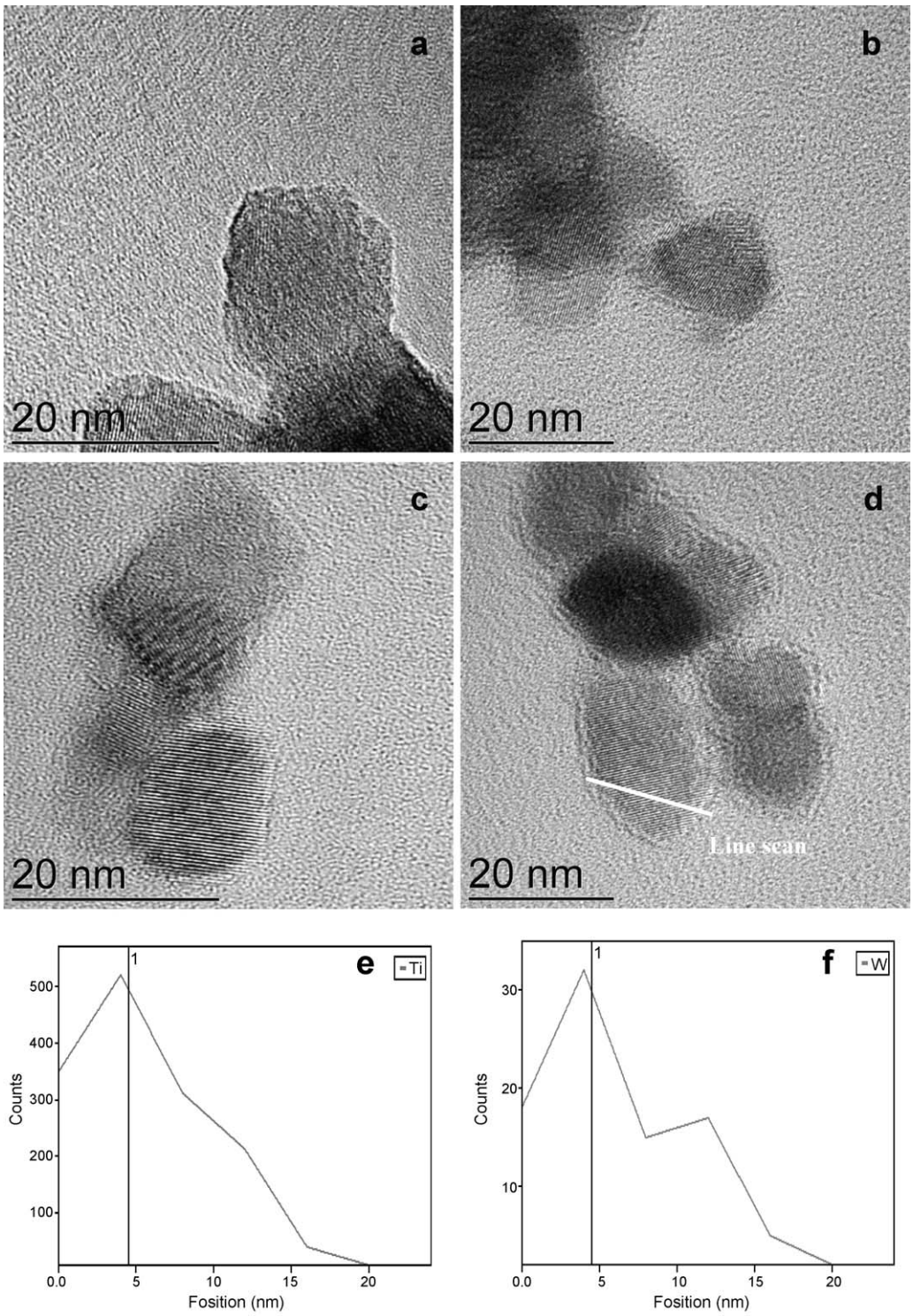

Fig. 5. HRTEM images of sol–gel nanocrystalline TiO_2 and $Ti(W)O_x$ powders calcined 15 h at 773 K: (a) TiO_2, (b) $Ti(W)O_x$-A(2), (c) $Ti(W)O_x$-B(2), (d) $Ti(W)O_x$-C(2), (e) Ti content, (f) W content determined by EDX (line scan through one particle of $Ti(W)O_x$-C(2)).

of detection, see Table 3; this sample also showed a low crystallite size (5 nm) and high SSA (217 m^2/g). Increase of calcination temperatures up to 873 K gave rise to an increase of crystallite size and a corresponding decrease of SSA. Highest activity was observed for the sol–gel sample calcined at 773 K. This constant improvement of activity from RT to 773 K can be explained by a constant increase of crystallite size up to ~14 nm. An effect of Cl^- ions at the surface of the particles cannot be excluded in regard of their concentration reported in Table 3. Indeed, samples as prepared and calcined up to 573 K present a high amount of Cl^- ions at the surface of the particles due to use of $TiCl_4$ as titanium precursor (one to two orders of magnitude higher than the sample calcined at 773 K). An additional step of washing samples several times in distilled water before calcination was done for photocatalysts calcined at 573 and 773 K. The sample washed and then calcined at 573 K showed a drastic increase of activity, while no

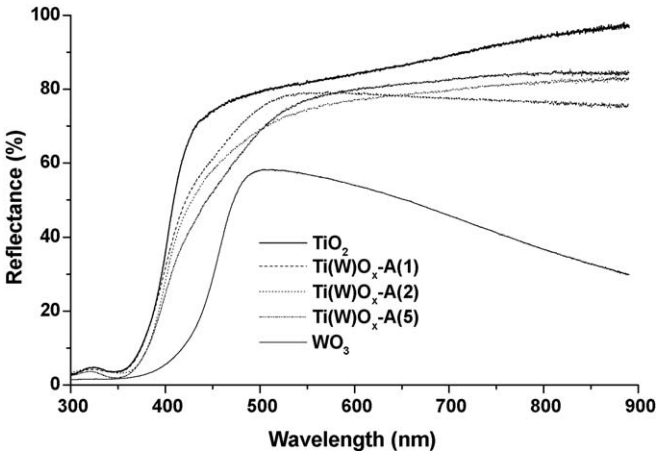

Fig. 6. Diffuse reflectance spectra of sol–gel TiO_2 and $Ti(W)O_x$-A series and pure WO_3 powders calcined 15 h at 773 K.

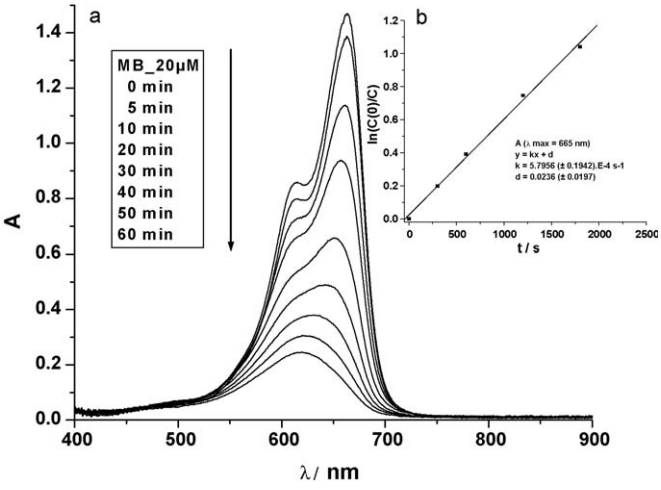

Fig. 7. (a) Typical UV–vis absorbance spectra obtained for the MB degradation under UVA irradiation for different time intervals. The spectra are obtained for $Ti(W)O_x$-A(2) sample calcined 15 h at 773 K. (b) Typical plot for determining the first order reaction rate constant *k*.

effect of the washing step was observed at 773 K. These results can be explained by the progressive removal of Cl^- by thermal treatment. Indeed, the amount of Cl^- decreases by a factor of 3 after washing in the case of the sample calcined at 573 K while no change is observed for the sample calcined at 773 K. In addition, the non-active photocatalysts do not show any visible adsorption of MB at the surface. The decrease in the rate of MB degradation in the presence of inorganic salts can be due to the formation of an inorganic salt layer at the surface of the particles, which inhibits the adsorption of MB molecules [43]. Higher calcination temperature leads to a progressive removal of Cl^- and an increase of crystallite size, both effects improve activity (the relative contribution of these parameters cannot be estimated from the measured data). Calcination temperature higher than 773 K leads to a major increase of crystallite size (>20 nm) and a strong decrease of activity. The same trend is observed for MB degradation under visible light, an optimum of activity is found for a calcination temperature of 773 K.

On the basis of the results presented above, TiO_2 and $Ti(W)O_x$ samples calcined at 773 K were chosen for the photocatalytic degradation of MB. The influence of W content and precursor on activity under UVA irradiation for $Ti(W)O_x$ samples is shown in Fig. 9 and Table 2. Addition of W considerably improves photocatalytic activity of the sol–gel samples even under UVA irradiation. A first explanation can be assigned to a decrease of crystallite size compare to pure TiO_2 accompanied by an increase of SSA of doped samples as reported in Table 2. Several authors [6] report a dependence of photocatalytic activity of MB degradation on the average nanocrystallite size of sol–gel samples with existence of a critical size around 15 nm. Below and above this size, the photocatalytic activity is observed to be reduced. It is also well known that an increase of SSA leads to an improvement of photocatalytic activity [1,5]. These observations are in good agreement with the results of photocatalytic activity presented in Table 2. The TiO_2 sample with a crystallite size >20 nm and a SSA of 16 m^2/g presents the lowest activity, while the doped $Ti(W)O_x$ samples with crystallite size <16 nm and a SSA >50 m^2/g show higher activity. A second explanation can be found in terms of electronic effect. Indeed, the doping substitution of Ti atoms by W atoms with higher-valence cations leads to an alteration of the electronic structure of the main semiconductor (TiO_2), which assists the charge separation efficiency, cf. Scheme 1. Therefore, W acts as an effective separation centre for electrons and holes. The photo-generated charge carriers can be transferred to different

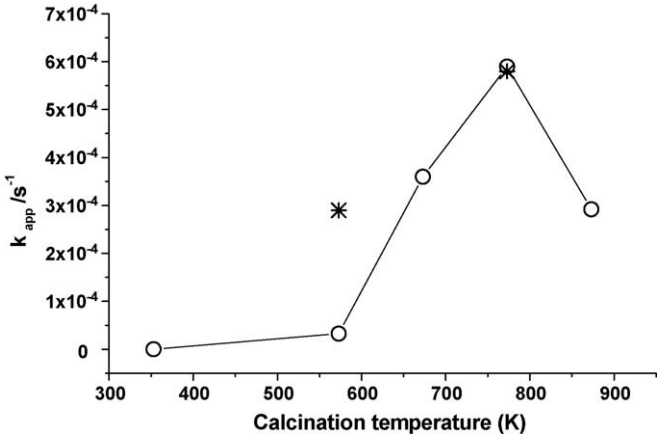

Fig. 8. Influence of the calcination temperature of $Ti(W)O_x$-A(2) sol–gel sample on MB photocatalytic degradation under UVA irradiation. (*) samples washed several times in distilled water before calcination.

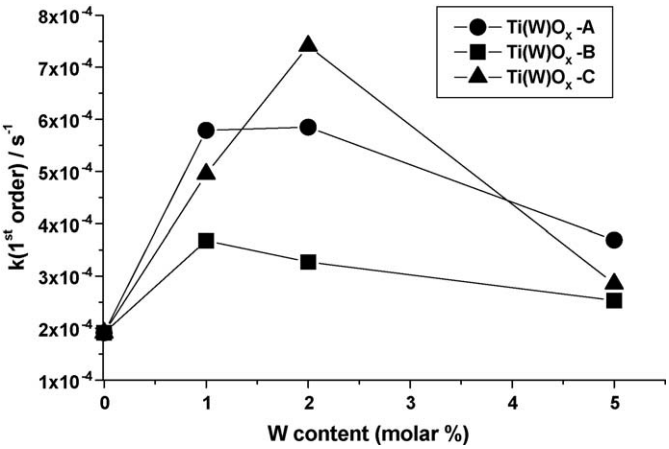

Fig. 9. Influence of W content on MB photocatalytic degradation under UVA irradiation for $Ti(W)O_x$ samples calcined at 773 K.

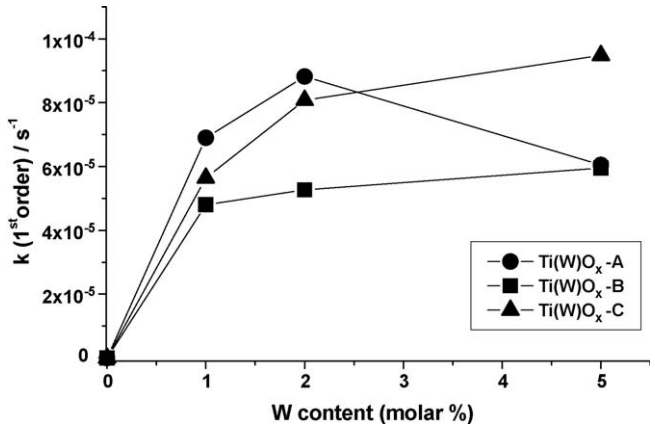

Fig. 10. Influence of W content on MB photocatalytic degradation under visible light irradiation for Ti(W)O_x samples calcined at 773 K.

surface sites where they will react with adsorbed species and enhance photocatalytic activity.Photocatalytic activity of Ti(W)O_x samples under UVA irradiation strongly depends on the W content and on the precursor choice. Ti(W)O_x-A and Ti(W)O_x-B present an optimum W amount between 1 and 2 mol%, while Ti(W)O_x-C shows a more pronounced dependence on W content with an optimum at 2 mol%. Increase of W content (5 mol%) leads to a decrease of UVA activity in all cases due to a dilution of the most active TiO_2 phase by the less active tungsten phase and a decrease of crystallite size (<12 nm). Regarding the nature of precursor, photocatalytic activity decreases in the following order: $WCl_6 > (NH_4)_6H_2W_{12}O_{40} > H_2WO_4$, for Ti(W)$O_x$ samples with a W content of 2 mol%. The samples using H_2WO_4 as W precursor exhibit a major decrease of activity. One reason for the strong decrease of photocatalytic activity might be pH change during the synthesis due to use of NH_4OH solution, inducing a deterioration of textural properties.

The influence of W content on activity under visible light irradiation for Ti(W)O_x samples synthesized with different precursors is shown in Fig. 10 and Table 2. Pure TiO_2 sample do not show any activity under visible light while all the doped Ti(W)O_x samples present some photocatalytic activity. The photocatalytic activity measure under visible light irradiation is around 10 times lower than the same activity measured under UVA irradiation. The photocatalytic activity under visible light irradiation can only be explained with the mention electronic effect: when W species are excited by visible light, holes will be formed in its valence band and can migrate to the valence band of TiO_2. Electrons generated in the valence band of TiO_2 can migrate to that of W. Finally, the holes accumulating in the TiO_2 can induce the photocatalytic oxidation reactions. Therefore, under visible light irradiation, photocatalytic activity is more sensitive to amount of W than crystallite size of nanoparticles. As expected, Ti(W)O_x-B and Ti(W)O_x-C are showing a continuous improvement of photocatalytic activity with increased W content even if crystallite size of samples with 5 mol% W is <12 nm. While, Ti(W)O_x-A shows an optimum in photocatalytic activity at 2 mol%, which decreases at higher W loadings. The photocatalytic activity of Ti(W)O_x samples with a W content of 2 mol% follows the order $(NH_4)_6H_2W_{12}O_{40} > WCl_6 > H_2WO_4$. As stated above, the lower activity of samples synthesized with H_2WO_4 precursor can be explained by change in the textural properties of these photocatalysts.

4. Conclusions

Nanocrystalline tungsten doped titania powders have been successfully synthesized by a sol–gel method based on hydrolysis of $TiCl_4$ in aqueous solution. Different W precursors and various W contents were used, aiming mainly at optimising their photocatalytic activities, as shown in the degradation of MB in aqueous solution under both UVA and visible light irradiation.

Addition of W drastically improves photocatalytic activity for both UVA and visible light irradiation. The doping substitution of Ti atoms by W atoms with higher-valence cations leads to an alteration of the electronic structure of the main semiconductor (TiO_2), which assists the charge separation efficiency. Highest activity is observed for sol–gel samples calcined at 773 K, due to full removal of Cl^- and increase of crystallite size. The dependence of photocatalytic activity on the crystallite size reveals the existence of a critical size around 15 nm under UVA irradiation. Activity of Ti(W)O_x sol–gel samples strongly depends on the tungsten content (maximum reached for a ratio between 1 and 2 mol%) and the precursor choice ($WCl_6 > (NH_4)_6H_2W_{12}O_{40} > H_2WO_4$) under UVA irradiation. Under visible-light, the electronic effects due to W addition are predominant and activity generally increases with W content.

The use of H_2WO_4 dissolved in NH_4OH solution as precursor of W dramatically decreases photocatalytic activity. This phenomenon might be explained by a pH change during synthesis affecting the textural properties of the photocatalysts.

Acknowledgements

The authors acknowledge the financial support from Austrian Nanoinitiative, BMVIT, FFG, FWF.

References

[1] M.R. Hoffmann, S.T. Martin, D.W. Bahnemann, Chem. Rev. 95 (1995) 69.
[2] A.L. Linsebigler, G. Lu, J.T. Yates, Chem. Rev. 95 (1995) 735.
[3] B. Tryba, A.W. Morawski, M. Inagaki, Appl. Catal. B: Environ. 46 (2003) 203.
[4] Y. Zheng, E. Shi, Z. Chen, W. Li, X. Hu, J. Mater. Chem. 11 (2001) 1547.
[5] J. Ryu, W. Choi, Environ. Sci. Technol. 42 (2008) 294.
[6] K.V. Baiju, S. Shukla, K.S. Sandhya, J. James, K.G.K. Warrier, J. Phys. Chem. C 111 (2007) 7612.
[7] D. Jiang, S. Zhang, H. Zhao, Environ. Sci. Technol. 41 (2007) 303.
[8] K. Dai, H. Chen, T. Peng, D. Ke, H. Yi, Chemosphere 69 (2007) 1361.
[9] F. Bosc, D. Edwards, N. Keller, V. Keller, A. Ayral, Thin Solid Films 495 (2006) 272.
[10] S. Ardizzone, C.L. Bianchi, G. Cappelletti, A. Naldoni, C. Pirola, Environ. Sci. Technol. 42 (2008) 6671.
[11] C.C. Wang, J.Y. Ying, Chem. Mater. 11 (1999) 3113.
[12] M.R. Mohammadi, M.C. Cordero-Cabrera, M. Ghorbani, D.J. Fray, J. Sol–Gel Sci. Technol. 40 (2006) 15.
[13] Y. Hu, H.L. Tsai, C.L. Huang, J. Eur. Ceram. Soc. 23 (2003) 691.
[14] A. Pottier, C. Chaneac, E. Tronc, L. Mazerolles, J. Jolivet, J. Mater. Chem. 11 (2001) 1116.
[15] S.J. Kim, S.D. Park, Y.H. Jeong, J. Am. Ceram. Soc. 82 (1999) 927.
[16] Y.V. Kolen'Ko, A.A. Burukhin, B.R. Churagulov, N.N. Oleynikov, Mater. Lett. 57 (2003) 1124.
[17] B. Li, X. Wang, M. Yan, L. Li, Mater. Chem. Phys. 78 (2002) 184.
[18] T. Sugimoto, X. Zhou, A. Muramatsu, J. Colloid Interf. Sci. 252 (2002) 339.
[19] M.A. Fox, M.T. Dulay, Chem. Rev. 93 (1993) 341.
[20] U. Diebold, Surf. Sci. Rep. 48 (2003) 53.
[21] M. Ksibi, M. Zemzemi, R. Boukchina, J. Photochem. Photobiol. A 159 (2003) 61.
[22] R. Asahi, T. Morikawa, T. Ohwaki, Science 293 (2001) 269.
[23] J.C. Yu, W. Ho, J.G. Yu, H. Yip, J.C. Wong, J.C. Zhao, Environ. Sci. Technol. 39 (2005) 1175.
[24] S.U.M. Khan, M. Al-Shahry, W.B. Ingler Jr., Science 297 (2002) 2243.
[25] J.C. Yu, J.G. Yu, W.K. Ho, Z.T. Jiang, L.Z. Zhang, Chem. Mater. 14 (2002) 3808.
[26] A. Kubacka, M. Fernandez-Garcia, G. Colon, J. Catal. 254 (2008) 272.
[27] K.M. Parida, Nruparaj Sahu, J. Mol. Catal. A 287 (2008) 149.
[28] A. Di Paola, G. Marci, L. Palmisano, M. Schiavello, K. Uosaki, S. Ikeda, B. Ohtani, J. Phys. Chem. B 106 (2002) 637.
[29] A. Di Paola, E. Garcia-Lopez, S. Ikeda, G. Marci, B. Ohtani, L. Palmisano, Catal. Today 75 (2002) 87.
[30] M. Bellardita, M. Addamo, A. Di Paola, L. Palmisano, Chem. Phys. 339 (2007) 94.
[31] H. Song, H. Jiang, X. Liu, G. Meng, J. Photochem. Photobiol. A 181 (2006) 421.
[32] F. Kiriakidou, D.I. Konkarides, X.E. Verykios, Catal. Today 54 (1999) 119.
[33] K.E. Karakitsou, X.E. Verykios, J. Phys. Chem. 97 (1993) 1184.
[34] Y. He, Z. Wu, L. Fu, C. Li, Y. Miao, L. Cao, H. Fan, B. Zou, Chem. Mater. 15 (2003) 4039.
[35] J. Papp, S. Soled, K. Dwight, A. Wold, Chem. Mater. 6 (1994) 496.
[36] C. Martin, G. Solana, V. Rives, G. Marci, L. Palmisano, A. Sclafani, Catal. Lett. 49 (1997) 235.

[37] G.N. Chaudhari, A.M. Bende, A.B. Bodade, S.S. Patil, V.S. Sapkal, Sens. Actuators B: Chem. 115 (2006) 297.
[38] A. Rampaul, I.P. Parkin, S.A. O'Neill, J. DeSouza, A. Mills, N. Elliott, Polyhedron 22 (2003) 35.
[39] S.Y. Chai, Y.J. Kim, W.I. Lee, J. Electroceram. 17 (2006) 909.
[40] K.K. Akurati, A. Vital, J.P. Dellemann, K. Michalow, T. Graule, D. Ferri, A. Baiker, Appl. Catal. B: Environ. 79 (2008) 53.
[41] H. Shinguu, M.M.H. Bhuiyan, T. Ikegami, K. Ebihara, Thin Solid Films 506 (2006) 111.
[42] M. Addamo, V. Augugliaro, A. Di Paola, E. Garcia-Lopez, V. Loddo, G. Marci, L. Palmisano, Colloid Surf. A 265 (2005) 23.
[43] C. Guillard, E. Puzenat, H. Lachheb, A. Houas, J.M. Herrmann, Int. J. Photoenergy 7 (2005) 1.
[44] S.S. Chan, I.E. Wachs, L.L. Murrell, J. Phys. Chem. 88 (1984) 5831.
[45] L.J. Alemany, L. Lietti, N. Ferlazzo, P. Forzatti, G. Busca, E. Giamello, F. Bregani, J. Catal. 155 (1995) 117.
[46] D.A. Tryk, A. Fujishima, K. Honda, Electrochim. Acta 45 (2000) 2363.
[47] A. Houas, H. Lachheb, M. Ksibi, E. Elaloui, C. Guillard, J.M. Herrmann, Appl. Catal. B: Environ. 31 (2001) 145.
[48] E.A. El-Sharkawy, A.Y. Soliman, K.M. Al-Amer, J. Colloid Interf. Sci. 310 (2007) 498.